Mesoporous silica as supports for Pd-catalyzed H₂O₂ direct synthesis: Effect of the textural properties of the support on the activity and selectivity

Elena Ghedini [a], Federica Menegazzo [a], Michela Signoretto [a], Maela Manzoli [b],
Francesco Pinna [a], Giorgio Strukul [a,*]

[a] Department of Chemistry, Cà Foscari University Venice and Consortium INSTM UdR Ve, Dorsoduro 2137, 30123 Venezia, Italy
[b] Department of Inorganic, Physical and Materials Chemistry, University of Torino, and NIS Centre of Excellence, via P. Giuria 7, 10125 Torino, Italy

ABSTRACT

Pd-based catalysts supported on commercial silica, SBA-15 and MCM-41 were tested for the direct synthesis of hydrogen peroxide under very mild conditions of temperature and pressure and outside the explosion range. Silica and SBA-15 impart good catalytic activity, selectivity, mechanical stability and reusability. Best results were obtained with SBA-15 samples that show higher productivity than plain silica. Further catalytic tests were performed at higher pressures, still outside the explosive region. Even under these reaction conditions, the SBA-15 catalysts are the most selective. Characterization data indicate a close correlation between the textural properties of the support and the catalytic activity of the examined samples. The mean Pd particle size observed on the SBA-15 is a good compromise between a high metal dispersion necessary for high catalytic activity and the presence of less energetic sites, on which O₂ can chemisorb without dissociation.

© 2010 Elsevier Inc. All rights reserved.

1. Introduction

Hydrogen peroxide is an excellent "green" oxidant but its relatively high cost has so far hampered a more general application of this commodity in the production of both fine and bulk chemicals. The development of a new, more economic process to synthesize H₂O₂ is considered to be a key step towards the introduction of new selective and sustainable oxidation processes [1]. In this respect, the direct H₂ + O₂ → H₂O₂ reaction will significantly reduce the environmental impact and may potentially halve the production cost of H₂O₂ in comparison with the current commercial process based on the methyl-anthraquinone route. The latter is economically profitable only when operated in large-scale plants, making the market a monopoly of a few producers. Several supported metal catalysts have been studied for the direct reaction, palladium, either alone or mixed with platinum [2–4] or gold [5–7], having emerged as the best option with respect to both activity and, very important for commercial applications, selectivity [8–10]. The latter is still unsatisfactory, and this drawback must be overcome for a possible successful industrial exploitation.

As shown in Scheme 1, there are four reactions, all catalyzed by palladium that are involved in the direct synthesis of H₂O₂, water formation being the most thermodynamically favored process.

Furthermore, because of the very broad explosion limits of H₂/O₂ gas mixtures (4–96%), the direct formation of H₂O₂ is regarded as potentially very hazardous, while operation under intrinsically safe conditions is very important for the viability of the process. Therefore, in spite of several published patents [11–17] and recent literature [18–24], at present no process for the direct synthesis of hydrogen peroxide has yet been marketed.

Many different supports have been investigated for this reaction, but the most common ones are silica [25] and carbon [26]. By comparing various supports, Edwards et al. have found that the nature of the support is an important factor for a successful reaction, observing, with carbon supported catalysts, high selectivity for the reaction (95%) in the absence of acid or halide promoters in the reaction medium. Carbon-supported Au–Pd alloy catalysts give the highest reactivity, while silica performed better than Al₂O₃ and Fe₂O₃ [22] under the same experimental conditions. Pd/SiO₂ catalysts have been extensively studied by Lunsford et al., albeit inside the explosive regime, proving useful candidates for the synthesis of hydrogen peroxide [4,24,27]. The influence of different halide ions on the performance of a Pd/SiO₂ sample in the direct H₂O₂ formation has also been reported [20]. In the present work, we have investigated the use of ordered mesoporous silica materials of the M41S family that was first successfully synthesized by the assembly of cationic surfactants with inorganic precursors in the early 1990s. Among these materials, MCM-41 and SBA-15 have received increasing scientific interest because of their

$$H_2 + O_2 \xrightarrow{\ -136\ kJ/mol\ ,\ k_1\ } H_2O_2 \xrightarrow{\ H_2\ k_3\ ,\ -211\ kJ/mol\ } H_2O$$
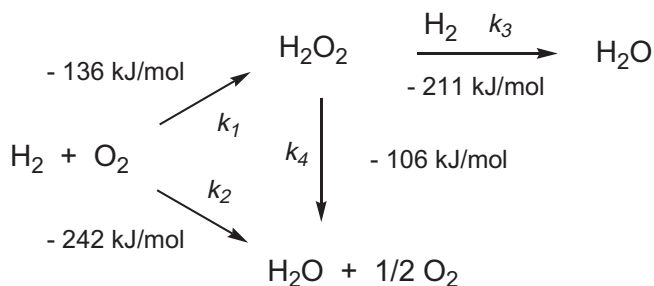
Scheme 1. Reaction network involved in H_2O_2 direct synthesis.

ordered channel structure, narrow pore size distribution, high surface area and pore volume that make them successful catalyst supports for a variety of reactions. In particular, SBA-15 is characterized by larger uniform pore size (4.7–30 nm), thicker silica walls (3–6 nm) and higher hydrothermal stability than MCM-41 [28]. The advantages of using ordered mesoporous solids in catalysis are related to the relatively large pores which facilitate mass transfer and the very high surface area which allows a high concentration of active sites per mass of material. In fact, a good heterogeneous catalyst must possess a pore structure capable to host the reagents and to allow the formation of the desired product. Consistently, metal nanoparticles deposited in porous and ordered host materials are desired for many practical applications and could be especially useful in a triphasic reaction with selectivity problems such as the H_2O_2 direct synthesis. The idea of the present work is to investigate the impact of mesopore confinement effects not only for reactants [29] but also for Pd effective dispersion. In particular, we aim at verifying whether geometry-dependent contributions can influence the catalytic behavior in hydrogen peroxide direct synthesis. For this purpose, we have prepared a series of palladium catalysts supported over commercial silica (Akzo) [30], MCM-41 and SBA-15, with different morphological properties. Herein, we describe the results obtained in hydrogen peroxide direct synthesis both under very mild conditions (1 bar and 293 K) and at higher pressure (10 bar) both to increase the productivity and to investigate the influence imparted by different silica supports in a wider range of conditions.

2. Experimental

2.1. Materials

All kinetic tests were performed in anhydrous methanol (Secco-Solv, Merck, $[H_2O] < 0.005\%$). Commercial standard solutions of $Na_2S_2O_3$ (Fixanal [0.01], Hydranal-solvent E, and Hydranal-titrant 2E, all from Riedel-de Haen) were used for iodometric and Karl-Fischer titrations.

2.2. Catalysts preparation

The MCM-41 mesoporous support was synthesized as previously reported [31]: a given amount of cetyltrimethylammonium bromide (CTABr, ALDRICH) was added to a NaOH aqueous solution and stirred slowly at room temperature for 40 min. The resulting solution was combined with tetraethylorthosilicate (TEOS, ALDRICH) as source of silica, and the reaction mixture was stirred at room temperature for 3 h. The gel was aged in static condition at 348 K for 72 h, then washed, dried at room temperature and finally calcined at 773 K for 6 h in air in order to remove the template [31].

SBA-15 was prepared with TEOS as the silicon source and EO20-PO70-EO20 (P123) (ALDRICH) as the template in an aqueous HCl solution [32,33], and then calcined at 773 K for 6 h in flowing air.

SiO$_2$ (Akzo) [30] has been used as received.

The three silica were impregnated by incipient wetness with H_2PdCl_4 aqueous solutions to give a nominal 1.5 or 2.5 wt% metal-loaded catalyst, and finally calcined again at 773 K in flowing air for 3 h.

2.3. Methods

Surface areas and pore size distributions were obtained from N_2 adsorption/desorption isotherms at 77 K (using a Micromeritics ASAP 2000 analyser). Surface area was calculated from the N_2 adsorption isotherm by the BET equation, and pore size distribution was determined by the BJH method [34]. Total pore volume was taken at $P/P_0 = 0.99$.

X-Ray diffraction patterns of the samples were obtained on a Philips PW 1820/00 instrument with Cu Kα radiation at 40 kV and 30 mA [33].

CO chemisorption measurements were performed at 298 K [35] using a lab-made pulse flow system. Prior to measurements, samples were subjected to a pretreatment involving exposure to hydrogen flow for 1 h at 298 K, followed by He purge for 2 h at the same temperature of reduction.

HRTEM analysis was performed on all catalysts using a Jeol JEM 3010 transmission electron microscope (300 kV) equipped with a side entry stage and a LaB$_6$ filament. The powdered samples supported on commercial silica were ultrasonically dispersed in isopropanol and the obtained suspension was deposited on a copper grid, coated with a porous carbon film. Moreover, a RMC ultramicrotome by Boeckeler equipped with a Power Tome PC was employed to prepare thin cross-sectional specimens of the samples embedded previously into a resin, to investigate the Pd dispersion inside the mesoporous channels of MCM-41 and SBA-15. These cross-sections were then deposited on the copper grids described earlier.

2.4. Catalyst testing

2.4.1. H_2O_2 direct synthesis at atmospheric pressure

Tests were carried out at atmospheric pressure in a thermostatted glass reactor (293 K) according to a previously described procedure [7,36]. Mixing was carried out with a Teflon®-made rotor operating at 1000 rpm. Oxygen and hydrogen were bubbled by a gas diffuser directly into the liquid phase with a total flow of 50 ml/min. A H_2:O_2 4:96 (nonexplosive and lower limit for nonflammable mixture [37]) gas mixture was used. The 0.03 M H_2SO_4 methanolic solution reaction medium (100 ml) was pre-saturated with the gas mixture before catalyst (135 mg) introduction. Samples were pre-activated in situ first by H_2 (15 min–30 cc/min) and then by O_2 (15 min–30 cc/min) flow to induce a Pd particle surface oxidation. During catalytic tests, small aliquots of the liquid phase were sampled through a septum and used for water and hydrogen peroxide determination. H_2O_2 concentration was measured by iodometric titration, whereas water was determined by volumetric Karl-Fischer method. The water content in the reaction medium before catalyst addition was determined prior to each catalytic experiment. H_2O_2 selectivity at time t was determined as follows:

$$S_{H_2O_2} = \frac{[H_2O_2]}{[H_2O_2] + [H_2O]}$$

2.4.2. H_2O_2 direct synthesis using an autoclave

Tests were performed at 293 K using an autoclave with a nominal volume of 250 ml. A 150 ml methanolic solution added with 250 µl of H_2SO_4 was used as the reaction medium. The water con-

tent in the reaction medium was determined prior to each catalytic experiment before catalyst (50 mg) introduction. Typically, the autoclave was charged, purged three times with CO_2 (10 atm) and then filled with the reactants to give a total pressure of 10 atm. A gas mixture with the following composition was used: $H_2:O_2:CO_2 = 3.6:7.2:89.2$ (nonexplosive and nonflammable mixture [37]). Mixing was carried out with a Teflon®-made rotor operating at 1200 rpm. Experiments were carried out for 30 min unless otherwise stated. Water and hydrogen peroxide contents were measured after each catalytic test as previously reported.

3. Results and discussion

3.1. Textural and chemical–physical properties of the supports

N_2 physisorption analyses were carried out in order to determine the surface area and pore size distribution of the supports. This point is crucial in this study as the choice of an appropriate mesoporous material can rule out mass transfer problems and at the same time allows a good dispersion of the Pd active phase. The adsorption isotherms of the three samples, as well as their BJH pore size distributions, are shown in Fig. 1, while the corresponding values are reported in Table 1. The MCM-41 sample shows an isotherm which is typical of materials with a similar pore size dimension ($\sim$3 nm) [38]. Such isotherm exhibits a significant adsorption at low relative pressure that is probably associated with a N_2 monolayer coverage of the pore walls. Another well-defined uptake step between $P/P_0 = 0.2$–0.3 can be associated with the filling of the mesopores due to capillary condensation. The sharpness of the latter step reflects a narrow and uniform pore size distribution as will be confirmed by transmission electron microscopy. SBA-15 exhibits a type IV isotherm with a clear type-H2 hysteresis loop that is typical of materials with cylindrical mesopores. The isotherm displays a sharp inflection occurring at relative pressure $0.7 < P/P_0 < 0.9$, corresponding to the capillary condensation in the mesopores which strongly suggests the presence of large pores (8 nm). The sharpness of this step indicates a uniform and narrow pore size which is in good agreement with the TEM results that will be discussed later. Also commercial silica presents a type IV isotherm with hysteresis loop typical of mesoporous materials. For this sample, a relatively low surface area can be calculated, at least with respect to the other solids, while its mean pore diameter is similar to that of the SBA-15 support.

Structure and morphology of the supports was investigated by X-ray diffraction and by transmission electron microscopy. The
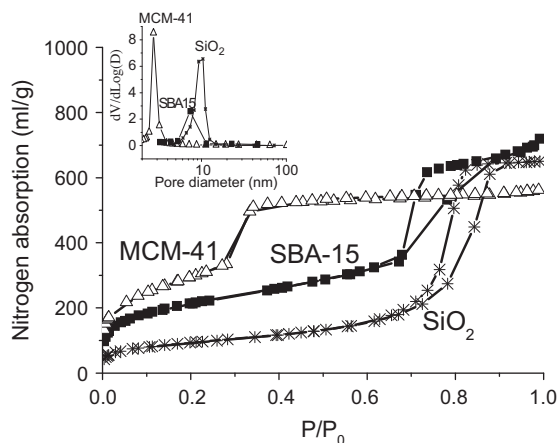
Table 1
Surface features of the supports after calcination.

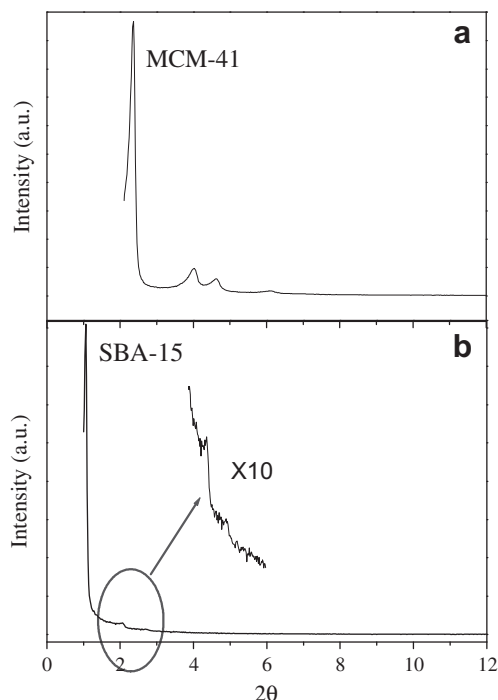| Support	Surface area (m²/g)	Pore diameter (nm)	Pore volume (cm³/g)
SBA-15	767	8.4	0.88
MCM-41	1072	2.9	0.87
SiO₂	331	9.1	1.01

Fig. 2. XRD patterns of calcined MCM-41 (section a) and SBA-15 (section b) supports.

low 2θ regions of the XRD powder spectra of the calcined supports are shown in Fig. 2. The MCM-41 system shows the typical XRD pattern of a mono-dimensional hexagonal meso-phase *p6mm* (section a) [31]. It exhibits a very intense diffraction peak and three other peaks that can be indexed, respectively, as the (1 0 0), (1 1 0), (2 0 0) and (2 1 0) reflections of the hexagonal structure. The high intensity and good resolution of XRD peaks, attributed to the regular arrangement of the periodic structure, indicate the high quality of the calcined MCM-41 sample [31]. The small angle XRD pattern of SBA-15 (Fig. 2, section B) is characterized by the presence of a prominent peak at $2\theta \sim 0.8°$ and of another weak peak around $2\theta \sim 1.8°$ that can be indexed as the (1 0 0) and (1 1 0) diffractions associated with the 2-D *p6mm* hexagonal symmetry. At low magnification, the TEM analyses of supports evidence that the MCM-41 is made of submicrometric particles that have mainly spherical shape (sometimes also rod-like). On the contrary, SBA-15 is composed of elongated/flat particles. Moreover, high-magnification TEM images of MCM-41 and of SBA-15 show the existence of both highly ordered hexagonal array and layered structural features (see Fig. 3). The hexagonal array corresponds to the view of the crystals down to the *c* axis while the layered image is that of the crystal whose *c* axis is parallel to the image plane. Images taken along the (0 0 1) direction (direction of the pore channel axis) clearly exhibit the uniform pore size and the hexagonal arrangement of the porous network, as clearly evidenced by the circle and the hexagon (Fig. 3, sections a and c). On the other hand, images taken along the (1 1 0) direction (perpendicular to the pore axis) show well-ordered channels with continuous pore
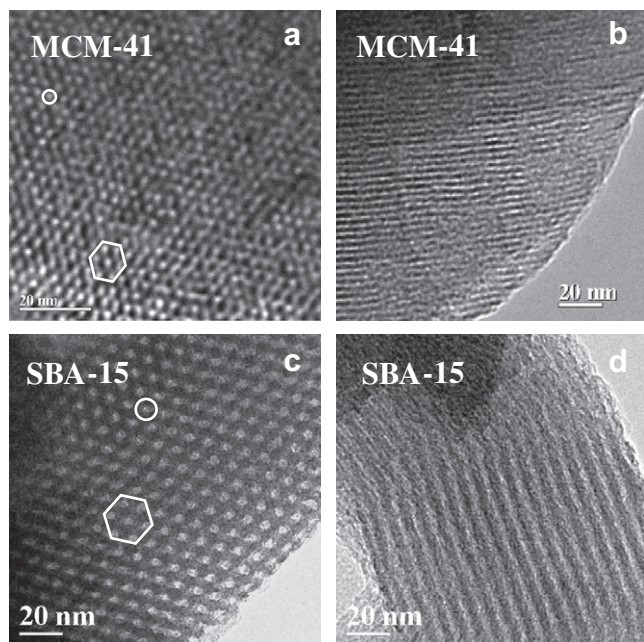

Fig. 1. N_2 physisorption isotherms of calcined supports and (insert) their BJH pore size distribution.

Fig. 3. High-magnification TEM images of MCM-41 and of SBA-15 taken along the (0 0 1) direction (sections a and c, where both uniform pores size and hexagonal arrangement of the porous network are evidenced by a circle and a hexagon) and acquired along the (1 1 0) direction (sections b and d, respectively).

walls (sections b and d, respectively). The pore sizes determined by TEM are in agreement with those obtained from N_2 adsorption, that is, around 3 nm in the case of the MCM-41 sample and 8–9 nm for the SBA-15 material.

3.2. Dispersion of the Pd phase

A TEM characterization was performed in order to investigate the Pd dispersion on supports. Studies were performed on the fresh (i.e. calcined) samples. Catalysts mildly reduced at 25 °C, like the samples produced *in situ* before the catalytic reaction, are morphologically very unstable under the 300 kV electron beam of the microscope (the temperature reached by the sample under observation is around 100–120 °C) hence no longer representative of the original sample. In Fig. 4, the Pd particle size distributions of 1.5Pd/SiO$_2$ (section a), 1.5Pd/MCM-41 (section b) and 1.5Pd/SBA-15 (section c) are compared. 1.5Pd/SiO$_2$ (section a) is characterized by a very heterogeneous dispersion of the metal: in particular, besides many small Pd particles (with average diameter of 2 nm) some agglomerates (with size ranging between 50 and 100 nm) and big "blocks" (with size ranging between 250 nm and 500 nm) are present. On the contrary, a large amount of small Pd nanoparticles with diameter lower than the pore size, i.e. 2.9 nm, has been detected inside the channels of MCM-41 during the observation of the cross-section specimen (Fig. 5, section a), as also shown by the Pd particle size distribution of 1.5Pd/MCM-41 (Fig. 4, section b and inset) where a large fraction of Pd particles fall below this critical value. These very small particles represent the 78.5% of the overall counted particles; however, big particles with diameter in the range of 10–60 nm but also up to 140 nm have also been observed. Hence, the largest fraction of the total Pd amount deposited on MCM-41 is outside the channels. In the case of 1.5Pd/SBA-15, we obtained a quite homogeneous Pd dispersion with respect to the other two samples. In particular, we found that almost the 90% of the counted particles is inside the pores, as evidenced by the dashed line in the inset of Fig. 4, section c. These Pd particles have a mean diameter of 4.5 nm. A TEM image, taken along the
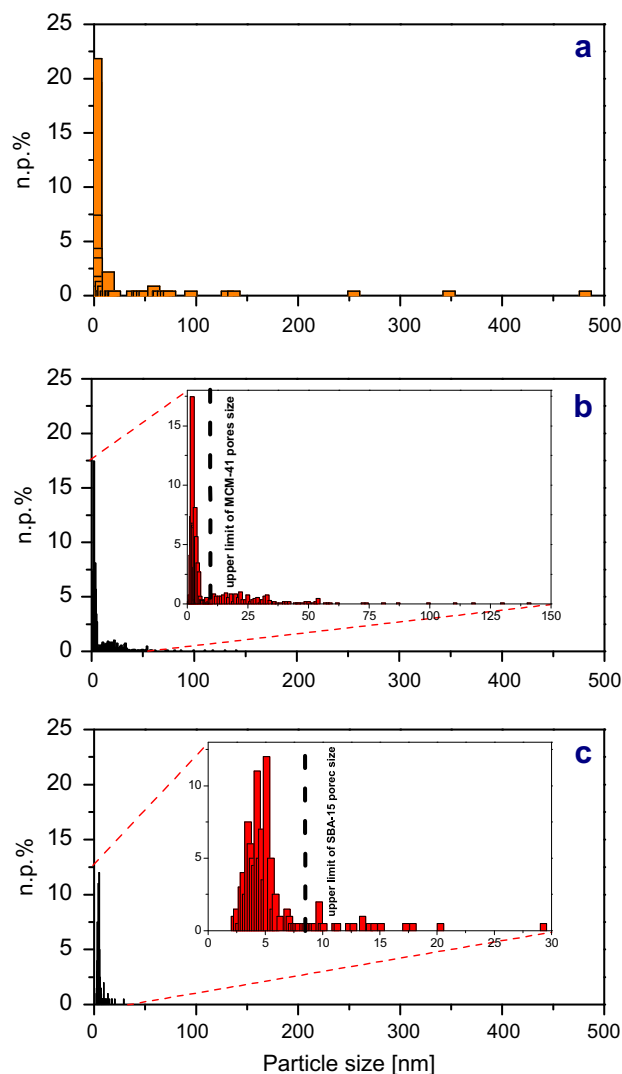

Fig. 4. Pd particle size distributions of 1.5Pd/SiO$_2$ (section a), 1.5Pd/MCM-41 (section b) and 1.5Pd/SBA-15 (section c). Dashed bars evidence the size of the mesoporous channels of 1.5Pd/MCM-41 and 1.5Pd/SBA-15 in the insets, where a zoom in the proper size ranges is shown.

(1 1 0) direction of the mesoporous silica, showing a typical Pd particle inside a channel, is reported in Fig. 5, section b. Moreover, only a small fraction of the Pd particles, mainly having size of 10–20 nm, is located outside. This feature clearly indicates that the vast majority of the total Pd loading is successfully placed inside the channels of SBA-15.

The dispersion of the samples with a higher Pd content (2.5 wt%) on the three different supports is lower than that found for the corresponding catalysts containing 1.5 wt% Pd (data not shown for the sake of brevity). The Pd particle size distributions of 2.5Pd/SBA-15, 2.5Pd/MCM-41 and 2.5Pd/SiO$_2$ have similar features compared to those previously discussed for 1.5Pd/SBA-15, 1.5Pd/MCM-41 and 1.5Pd/SiO$_2$, with the same heterogeneous dispersion observed in the Pd/SiO$_2$ sample, an even larger amount of Pd located outside the pores in Pd/MCM-41 and Pd located mostly inside the pores in Pd/SBA-15, but all sizes shifted towards higher values.

Besides HRTEM analyses, we have determined Pd dispersion by pulse flow CO chemisorption measurements [30,35,39]. We have chosen to perform such characterizations on mildly reduced catalysts, in order to mimic the same reductive pretreatment of the cat-
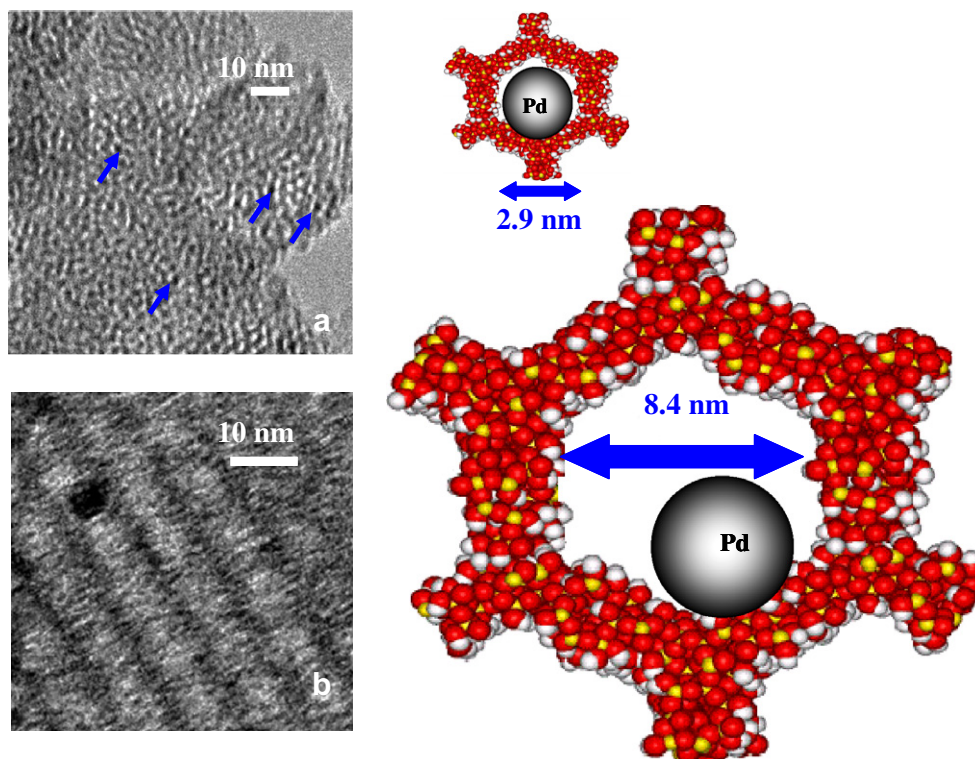
Fig. 5. . HRTEM image of a Pd particle inside a channel taken along the (1 1 0) direction of MCM-41 (section a) and of SBA-15 (section b). On the right, schematic representation of the pores size of the mesoporous systems. Original magnification: 120,000× and 100,000×, respectively.

Table 2
Chemisorption values and productivity after 5 h of reaction at atmospheric pressure.

	$mLCO_{(273K)}/g_{Pd}$	Productivity ($mmol_{H2O2}/g_{Pd}h$)
1.5Pd/SiO$_2$	23	762
1.5Pd/MCM-41	49	479
1.5Pd/SBA-15	42	1134
2.5Pd/SiO$_2$	29	443
2.5Pd/MCM-41	34	415
2.5Pd/SBA-15	32	800

alytic reaction and determine in such a way the amount of active sites that are actually present during the reaction. As previously demonstrated by TEM distributions, some samples are characterized by a very heterogeneous dispersion, which makes the assumption of a uniform Pd/CO chemisorption stoichiometry not reliable, hence only the experimental values ($mLCO_{(273K)}/g_{Pd}$) have been reported in Table 2.

The chemisorption results show that CO adsorbed in both MCM-41 supported catalysts is higher than the corresponding samples over SBA-15 and commercial silica, indicating that in these samples the total adsorbing sites are more abundant and metal dispersion is higher. Such chemisorption data agree with the TEM results previously discussed.

3.3. Catalytic data

In order to investigate the above materials as catalysts for a safe and potentially cheap H_2O_2 production, some tests were carried out under very mild conditions (1 bar and 293 K) and outside the explosive region employing surface oxidized Pd^0 catalysts, which have already proved advantageous for catalytic activity and selectivity [7]. This pretreatment is as follows: samples are reduced *in situ* by passing a pure hydrogen flow into the reaction medium, leading to a completely reduced catalyst. Then, pure oxygen is fed.

Excess oxygen is removed by passing pure nitrogen. The undiluted hydrogen/oxygen mixture used for catalytic tests allows maintaining the sample surface oxidized [7]. Reactions were carried out in methanol, which is the solvent of choice for many oxidation processes involving H_2O_2 and the best solvent for H_2O_2 direct synthesis, as previously reported [36]. Fig. 6 shows the comparison of the catalytic performance in H_2O_2 formation (left) and selectivity (right) among the different catalysts. Samples supported on commercial silica (1.5Pd/SiO$_2$ and 2.5P/SiO$_2$) show a linear increase in hydrogen peroxide formation with time and a constant selectivity during 5 h of reaction. An identical behavior is displayed by the samples supported on SBA-15 (1.5Pd/SBA-15 and 2.5Pd/SBA-15) albeit with a higher hydrogen peroxide production than the corresponding Pd/SiO$_2$ samples, as well as a higher productivity as evidenced by the values reported in Table 2. In addition, the SBA-15 samples present constant selectivity with profiles that are almost superimposable to those of the corresponding Pd/SiO$_2$ catalysts (both in the 60–65% range).

A completely different behavior has been found for the two MCM-41 supported catalysts. The profiles of the H_2O_2 concentration are linear only for the first 3 h of reaction, and then both productivity and selectivity slow down.

The different productivity and selectivity profiles observed in Fig. 6 for Pd/SiO$_2$ and Pd/SBA-15 on the one side and Pd/MCM-41 on the other side are indicative of a different relative weight of the four reactions indicated Scheme 1. While for the former catalysts the linear H_2O_2 and H_2O (not shown) formation and the constant selectivity are clearly indicative of the presence of two parallel reactions where the contribution by consecutive processes is negligible (k_3 and k_4 are negligible with respect to k_1 and k_2) with the latter catalysts the shape of the H_2O_2 profile and the declining selectivity suggest that consecutive processes play a significant role. These aspects have been already addressed in the past by analysis of the kinetic constants [7,36,45,46].
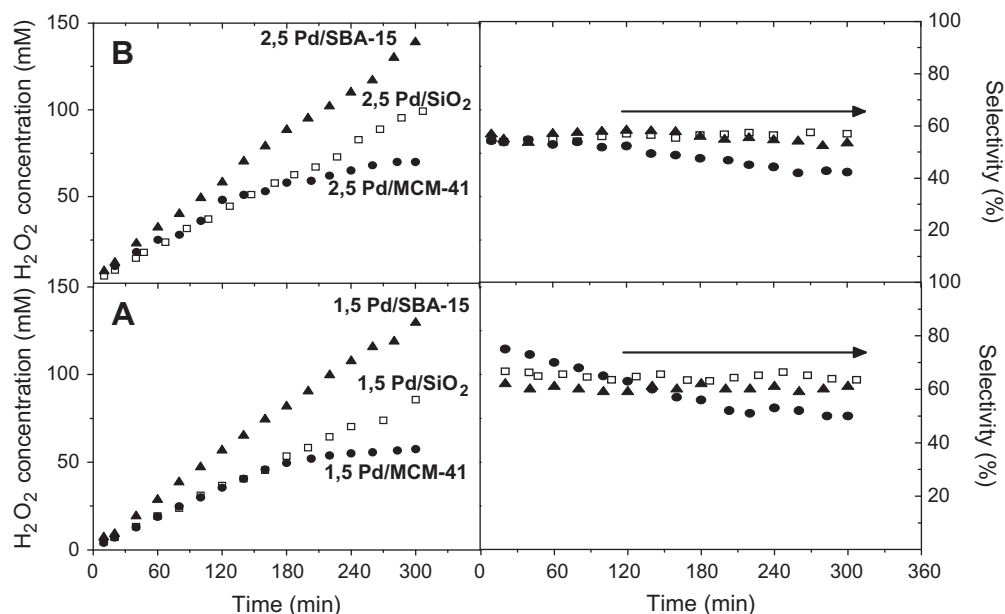
Fig. 6. H_2O_2 production (left) and selectivity (right) for catalytic tests at atmospheric pressure and room temperature for 1.5 wt%Pd (A) and 2.5 wt%Pd (B) samples.

Our best catalysts (Pd/SiO$_2$ and Pd/SBA-15) were also tested for recycling showing identical activity and selectivity, while at the same time no activity was observed when recycling the liquid phase after catalyst filtration. Pd analysis on the used samples indicates that differences with respect to the fresh catalysts are within the experimental error. All these observations are strongly indicative that no metal leaching occurred during catalytic experiments.

With the aim of further improving the productivity, catalytic tests were performed also at higher pressures, still working outside the explosive region, at room temperature and without halides addition. CO$_2$ was used as diluent inert gas because the explosive region for H$_2$/O$_2$ mixtures is narrower than that for other inert gases [40] and its acidity could help improve hydrogen peroxide

stability. Carbon dioxide is generally considered to be environmentally benign since it is naturally abundant, relatively non-toxic and nonflammable [40,41]. As reported in Fig. 7, productivities at $P = 10$ bar are obviously higher than that at $P = 1$ bar for all the examined catalysts and are similar for the three supports. The most important result is the highest selectivity of the SBA-15 supported catalyst.

4. Discussion

The data reported in Section 3 indicate a close correlation between textural properties of the samples and their catalytic activity, showing that surface area, pore size distribution and metal dispersion of the catalysts have a key role on directing the course of reaction. We have already discussed [42] that oxygen adsorption without dissociation is a necessary condition to hydrogen peroxide formation and it is strictly correlated with the nature of the adsorbing Pd sites that can be more or less energetic. In particular, chemisorption on nondefective (less energetic) sites takes place without dissociation and, at the same time, more energetic sites like defects, edges, corners that are the most abundant on small Pd particles, will dissociatively chemisorb O$_2$. In this respect, the results here reported demonstrate that the size of the support channels plays a crucial role in determining a homogeneous Pd size distribution. Catalytic data evidenced a poor activity and selectivity for the 1.5Pd/MCM-41 sample that contains a large amount of Pd nanoparticles with size of about 2 nm along with a fraction of large particles lying outside the support channels that is small in number but large in weight. The results here reported confirm that if the size of Pd is small, the metal is very active due the presence of more energetic Pd sites but the selectivity drops down. At the same time, the contribution of the big particles is negligible [43]. As summarized in Scheme 2, the MCM-41 support presents narrow pores and some Pd particles could even hamper the way through the pores. In practice, the main advantage of the highest surface area is wasted, because the largest Pd amount is located outside the pores and agglomerated in very large, catalytically useless particles. Besides the thin wall thickness of the MCM-41 [44] renders it extremely sensitive towards stability problems, being partly responsible of the selectivity drop. On the contrary, the thick wall
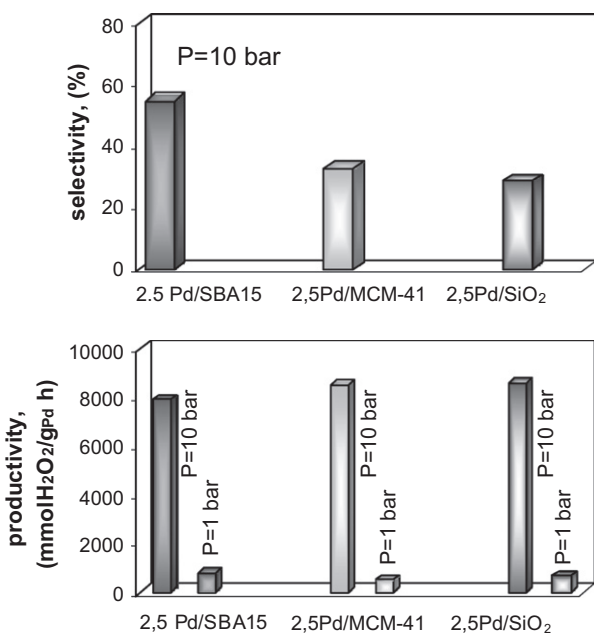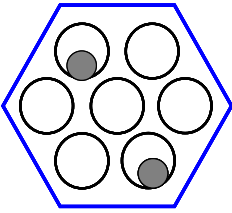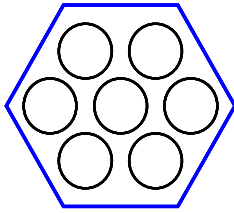

Fig. 7. H$_2$O$_2$ productivity (lower section) and selectivity after 30 min of reaction (upper section) for H$_2$O$_2$ direct synthesis performed at 10 bar.

Catalyst	Support pores diameter	Pd particles dispersion	Energetic Pd sites	H$_2$O$_2$ selectivity productivity
Pd/MCM-41	MCM-41, 2.9 nm	average diameter: about **2 nm** 78.5% of the counted particles inside the pores. **The largest amount of Pd is outside the channels.**	yes O$_2$ dissociation	↓ ↓
Pd/SBA-15	SBA-15, 8.4 nm	average diameter: about **4.5 nm** almost 90% of the counted particles inside the pores. **The largest amount of Pd is inside the channels.**	no O$_2$ activation without dissociation	↑ ↑

Scheme 2. Characterization data and catalytic performances of the examined catalysts.

thickness [28] of the SBA-15 supported catalysts allows a good mechanical stability and reusability. Both samples supported on SBA-15 have very good catalytic performance in terms of activity and selectivity, and show better results than those previously obtained in the same experimental conditions with both mono and bimetallic Pd active phases on different supports [7,36,45,46]. TEM results have shown that the SBA-15 support is the most suitable to obtain a catalyst in which the Pd average diameter (4.5 nm) is the right compromise between a high dispersion and the presence of less energetic sites to avoid a drop in selectivity, according to our previous results [42] and where almost 90% of the palladium present is usefully located inside the pores. Despite this feature, as depicted in Scheme 2, the pore size of the SBA-15 material is sufficiently large to allow also an easy diffusion of reagents and products.

In summary, the nature of SBA-15 material ensures to these Pd catalysts the mechanical stability and reusability properties that are necessary requirements on the way to practical applications and, more importantly, its uniform, relatively large mesoporosity seems particularly appropriate to ensure the palladium particles the right morphology to maximize both activity and selectivity in hydrogen peroxide formation.

5. Conclusions

Pd-based samples supported on silica were successfully tested for the direct synthesis of hydrogen peroxide outside the explosion range even under very mild conditions (1 bar and 293 K). The ability of the SBA-15 support to influence the final Pd particles dispersion makes it the best support for this reaction, even if compared with previously investigated catalysts [7,36,45,46]. In SBA-15, besides the thick wall thickness that makes it stable in the reactor, the pore size is sufficiently large to accommodate the vast majority of the metal inside the pores avoiding the formation of catalytically inactive Pd particles and the average particle size that can be formulated on this support is the most appropriate. Although, in general, metal dispersion, namely the ratio between surface and total metal atoms, is a critical factor in many catalytic reactions and should be as high as possible, in this process this is not the case. In fact, the size of Pd particles observed inside SBA-15 is the ideal compromise to cope with two opposing trends: a high metal dispersion leading to high activity and the presence of less energetic sites, on which O$_2$ can chemisorb without dissociation.

References

[1] G. Centi, S. Perathoner, Selective Oxidation Industrial, in: I.T. Horvath (Ed.), Encyclopedia of Catalysis, Vol. 6, J. Wiley & Sons Pub, New York, 2003, pp. 239–299.
[2] S. Abate, S. Melada, G. Centi, S. Perathoner, F. Pinna, G. Strukul, Catal. Today 117 (2006) 193.
[3] V.R. Choudhary, C. Samanta, T.V. Choudhary, Appl. Catal. A – Gen. 308 (2006) 128.
[4] Q. Liu, J.C. Bauer, R.E. Schaak, J.H. Lunsford, Appl. Catal. A – Gen. 339 (2008) 130.
[5] Landon, P.J. Collier, A.J. Papworth, C.J. Kiely, G.J. Hutchings, Chem. Commun. (2002) 2058.
[6] G.J. Hutchings, Chem. Commun. 10 (2008) 1133.
[7] F. Menegazzo, P. Burti, M. Signoretto, M. Manzoli, S. Vankova, F. Boccuzzi, F. Pinna, G. Strukul, J. Catal. 257 (2008) 369.
[8] T.A. Pospelova, N.I. Kobozev, Russ. J. Phys. Chem. 35 (1961) 262.
[9] J.M. Campos-Martin, G. Blanco-Brieva, J.L.G. Fierro, Angew. Chem. Int. Ed. 45 (2006) 6962.
[10] Q. Liu, J.C. Bauer, R.E. Schaak, J.H. Lunsford, Angew. Chem. Int. Ed. 47 (2008) 6221.
[11] H.-J. Riedl, G. Pfleiderer, US 2215883, 1940.
[12] L.W. Gosser, US 4681751, 1987.
[13] L.W. Gosser, J.T. Schwartz, US 4772485, 1988.
[14] J. Van Weynbergh, J.-P. Schoebrechts, US 5447706, 1995.
[15] B. Bertsch-Frank, I. Hemme, S. Katusic, J. Rollmann, US 6387364, 2002.
[16] G. Paparatto, R. D'Aloisio, G. De Alberti, R. Buzzoni, US 6630118, 2003.
[17] K.M. Vanden Bussche, S.F. Abdo, A.R. Oroskar, US 6713036, 2004.
[18] R. Burch, P.R. Ellis, Appl. Catal. B – Environ. 42 (2003) 203.
[19] V.R. Choudhary, P. Jana, J. Catal. 246 (2007) 434.
[20] C. Samanta, V.R. Choudhary, Catal. Commun. 8 (2007) 2222.
[21] A. Herzing, A.F. Carley, J. Edwards, G.J. Hutchings, C.J. Kiely, Chem. Mater. 20 (2008) 1492.
[22] J.K. Edwards, A. Thomas, B. Solsona, P. Landon, A.F. Carley, G. Hutchings, Catal. Today 122 (2007) 397.
[23] D. Hancu, E.J. Beckman, Green Chem. 3 (2001) 80.
[24] Q. Liu, J.H. Lunsford, J. Catal. 239 (2006) 237.
[25] Q. Liu, K. Gath, J.C. Bauer, R.E. Schaak, J.H. Lunsford, Catal. Lett. 132 (2009) 342.
[26] J. Edwards, B. Solsona, E. Ntainjua, A.F. Carley, A. Herzing, C. Kiely, G. Hutchings, Science 323 (2009) 1037.
[27] Y. Han, J.H. Lunsford, J. Catal. 230 (2005) 313.
[28] D. Zhao, Q. Huo, J. Feng, B.F. Chmelka, G.D. Stucky, J. Am. Chem. Soc. 120 (1998) 6024.
[29] S. Pariente, P. Trens, F. Fajula, F. Di Renzo, N. Tanchoux, Appl. Catal. A – Gen. 307 (2006) 51.
[30] P. Canton, F. Menegazzo, S. Polizzi, F. Pinna, N. Pernicone, P. Riello, G. Fagherazzi, Catal. Lett. 88 (2003) 141.

[31] E. Ghedini, M. Signoretto, F. Pinna, G. Cerrato, C. Morterra, Appl. Catal. B – Environ. 67 (2006) 24.
[32] D. Zhao, J. Feng, Q. Huo, N. Melosh, G.H. Frederickson, B.F. Chmelka, G.D. Stucky, Science 279 (1998) 548.
[33] E. Ghedini, M. Signoretto, F. Pinna, G. Cruciani, Catal. Lett. 125 (2008) 359.
[34] S.J. Gregg, K.S.W. Sing, Adsorption, Surface Area and Porosity, second ed., Academic Press, 1982. p. 111.
[35] G. Fagherazzi, P. Canton, P. Riello, N. Pernicone, F. Pinna, M. Battagliarin, Langmuir 16 (2000) 4539.
[36] S. Melada, R. Rioda, F. Menegazzo, F. Pinna, G. Strukul, J. Catal. 239 (2006) 422.
[37] B. Lewis, G. von Elbe, Combustion, Flames and Explosion of Gases, Academic Press, New York and London, 1961.
[38] X.S. Zhao, G.Q. Lu, A.K. Whittaker, G.J. Millar, H.Y. Zhu, J. Phys. Chem. B 101 (1997) 6525.
[39] P. Canton, G. Fagherazzi, M. Battagliarin, F. Menegazzo, F. Pinna, N. Pernicone, Langmuir 18 (2002) 6530.
[40] J.K. Edwards, B. Solsona, P. Landon, A.F. Carley, A. Herzing, C. Kiely, G. Hutchings, J. Catal. 236 (2005) 69.
[41] E.J. Beckman, Green Chem. 5 (2003) 332.
[42] S. Abate, G. Centi, S. Melada, S. Perathoner, F. Pinna, G. Strukul, Catal. Today 104 (2005) 323.
[43] S. Melada, F. Pinna, G. Strukul, S. Perathoner, G. Centi, J. Catal. 235 (2005) 241.
[44] P. Selvam, S.K. Bhatia, C.G. Sonwane, Ind. Eng. Chem. Res. 40 (2001) 3237.
[45] F. Menegazzo, M. Signoretto, M. Manzoli, F. Boccuzzi, G. Cruciani, F. Pinna, G. Strukul, J. Catal. 268 (2009) 122.
[46] G. Bernardotto, F. Menegazzo, F. Pinna, M. Signoretto, G. Cruciani, G. Strukul, Appl. Catal. A – Gen. 358 (2009) 129.